Site-selective spectroscopy of $CaF_2:Ho^{3+}$

M. B. Seelbinder and J. C. Wright
Department of Chemistry, University of Wisconsin, Madison, Wisconsin 53706
(Received 13 June 1979)

Using selective laser excitation, the crystallographic sites arising from fluoride compensation of Ho^{3+} doped into CaF_2 have been investigated. Two sites are found corresponding to single-Ho^{3+}–single-fluoride-interstitial pairs. These sites are suspected to be the tetragonal and trigonal sites observed in the similar $CaF_2:Er^{3+}$ system. Two sites and a family of similar sites are found to be dimers and/or higher-order clusters. These sites exhibit upconversion and energy-transfer-assisted decay characteristics of the closely coupled rare-earth ions. This phenomenon was used to observe energy transfer between an Er^{3+} and a Ho^{3+} in a double-doped crystal, and therefore show the equivalency of the respective sites in each of the ion's individual spectra.

There have been a number of experiments with trivalent rare-earth ions doped into fluorite lattices which show that the population of rare-earth ions in the different crystallographic sites caused by charge compensation is a function of both the specific rare-earth dopant ion and the specific lattice. Early investigations by Sierro[1] showed that Gd^{3+} doped into a BaF_2 lattice produced a site of trigonal symmetry, where a fluoride interstitial compensates the Gd^{3+} in a second-nearest-neighbor interstitial position. No Gd^{3+} ions in the tetragonal symmetry sites, expected for first-nearest-neighbor compensation, were seen. A systematic investigation by Ranon and Yariv[2] involving Yb^{3+} in BaF_2, SrF_2, and CaF_2 found that BaF_2 along with SrF_2 lattices had only the trigonal symmetry sites, while CaF_2 had both trigonal and tetragonal sites. Brown and co-workers[3] studied the site distribution as the dopant ion increased in atomic number across the periodic table. They found that Ce^{3+}, Nd^{3+}, and Sm^{3+} in SrF_2 produced only tetragonal symmetry sites, Gd^{3+} and Dy^{3+} produced both tetragonal and trigonal sites, and Er^{3+} and Yb^{3+} produced only trigonal sites. Additionally, in the Er^{3+}-doped lattices, they identified cubic-symmetry sites where the fluoride-interstitial charge compensation is distant. As the dopant concentration was increased from 0.02 mole% to 1.0 mole%, the cubic site concentration first decreased, but then increased.

Fong, Ford, and Heist[4] proposed that the importance of the site of the dopant ion relative to the host lattice ion could be accounted for by the degree of displacement polarization introduced into the lattice by the substitution. This polarization results because the size mismatch creates an elastic displacement and alters the binding energy of the various impurity-defect pairs. This situation would predict that as the ion size of the rare-earth dopant decreases, the trigonal site would become favored at the expense of the tetragonal site. Weber and Bierig[5] similarly hypothesized that rare-earth ions in the second half of the periodic table would actually favor cubic compensation. Catlow[6] has calculated the lattice strain and has been able to satisfactorily explain the trend from predominantly trigonal sites in BaF_2 and SrF_2 lattices to a roughly equal number of trigonal and tetragonal sites in CaF_2.

At higher concentrations of dopant, the site behavior becomes more difficult to describe. Naberhuis and Fong[7] developed a model which predicted the presence and importance of $(R^{3+}-F^-)_2$, dimers, in the crystal equilibrium at higher concentrations. Their theory also predicted that trimers and higher-order clusters would not be present in significant numbers. Much experimental work confirms these ideas. Recent work using methods of ^{19}F NMR,[8] ionic thermoconductivity,[9] and selective laser excitation[10] shows that above a tenth of a mole percent, the dominant crystallographic sites arise from clusters of two or more rare-earth fluoride-interstitial pairs. Recent models show that the clustering controls all of the solid-state equilibrium.[11,12,17]

The presence of well-defined dimer and cluster sites in CaF_2 is interesting from the viewpoint of both performing fundamental studies[14] and using the sites for analytical chemical measurements.[15] The small separation between the ions in these sites promotes very efficient energy transfer. The absence of energy transfer to more distant ions and the well-defined nature of the ionic arrangement means that unique energy-transfer rates can be directly obtained from experiment without resorting to the necessity of modeling the radial dependence of the rates.[16] In order to make effective use of this situation, it is necessary to have clusters comprised of more than one type of ion. Since the different ionic radii can cause pronounced changes in the site distribution, it becomes necessary to predict what these changes will be in order

to effectively use the system.

It is expected that the dimer and cluster site populations depend on the ionic radius of the dopant ion relative to the lattice just as for the sites having one rare-earth ion with its associated charge compensating fluoride interstitial (single pair sites). Therefore, a systematic change in site population should be observed across the rare earths as in the single pair sites. For single pair sites, correlation of a particular site from dopant to dopant has been accomplished using NMR-optical, ESR-optical, or optical Zeeman experiments; but the cluster sites cannot be done as easily with these techniques. This paper presents an optical method of correlation of a particular cluster site of one rare-earth dopant with that of a different rare-earth dopant. It represents the first step in accomplishing an understanding of the site distribution systematics. The method of selective laser excitation[10] is used to obtain the single pair and cluster site distributions of Ho^{3+} doped into CaF_2 at two concentrations. A method of identifying one of the cluster sites in the CaF_2: Ho^{3+} as corresponding to a cluster site observed in CaF_2: Er^{3+} is presented. Spectral and temporal characteristics of the CaF_2: Ho^{3+} sites will be discussed for observed lines in both absorption (excitation) spectra and fluorescence spectra.

EXPERIMENTAL PROCEDURE AND RESULTS

General

The energy level diagram for the Ho^{3+} 4f electron configuration[10] is shown in Fig. 1. Our system is capable of selectively exciting manifolds D through J from the ground state, and able to detect resulting fluorescence from the near uv to the near ir.

The optical spectrum obtained from Ho^{3+} is much more complex than that from Er^{3+} due to its non-Kramers ion character. Therefore, $2J+1$ lines are present in Ho^{3+} for each single ion site, as opposed to the $(2J+1)/2$ lines predicted and observed in a Kramers ion such as Er^{3+}.

CaF_2: 0.01-mole % Ho^{3+}

The absorption spectrum of the electronic manifolds in a CaF_2: 0.01-mole % Ho^{3+} crystal is characterized by a small number of very sharp absorption lines. The maximum number of lines that can be observed for a given J manifold is the product of the number of sites and the number of crystal field levels per site, $2J+1$. An example of an absorption spectrum is shown in Fig. 2 for the ${}^5I_8 \rightarrow {}^5F_5$ transition. By tuning the dye laser to a particular absorption line, a fluorescence spectrum can be obtained that is characteristic of the

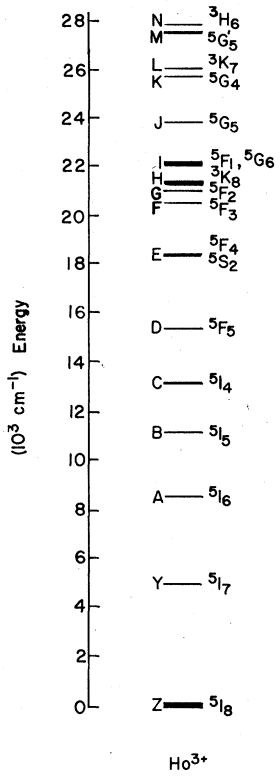

FIG. 1. Energy-level diagram of the $4f$ electrons in Ho^{3+}.

Ho^{3+} site whose absorption has been excited. The fluorescence spectrum obtained by exciting the absorption line at 637.5 nm in Fig. 2 is shown in Fig. 3.

If now the fluorescence line at 644 nm in Fig. 3 is monitored as the dye laser is scanned, an excitation spectrum is produced that is associated with the site having that particular fluorescence transition. This procedure isolates the lines in the absorption spectra that are associated with a particular site. Repeating these two steps for each absorption (excitation) and fluorescence line establishes the correspondence between the different sites present in the crystal, the absorption

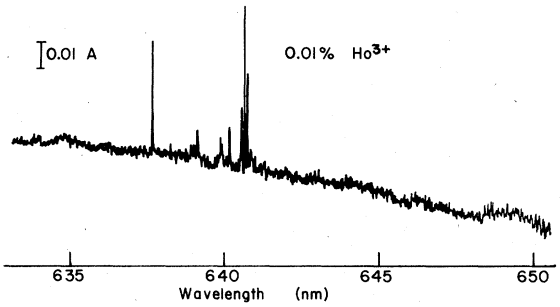

FIG. 2. ${}^5I_8 \rightarrow {}^5F_5$ ($Z \rightarrow D$) absorption spectrum of 0.01-mole % Ho^{3+} in CaF_2. Ordinate in absorbance units (A).

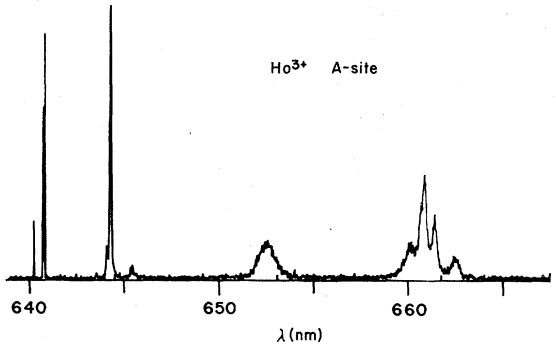

FIG. 3. A site fluorescence spectrum: ${}^5F_5 \rightarrow {}^5I_8$ ($D \rightarrow Z$).

spectra, and the respective excitation and fluorescence spectra.

When this process is carried out for all the manifolds in the CaF_2: Ho^{3+} crystal, it is found that all the absorption lines can be orgainzed into two groups corresponding to two different crystallographic sites for the Ho^{3+} ion. These sites are labeled A and B to facilitate discussion and follow the pattern observed in 0.01-mole% CaF_2: Er^{3+} crystals, where the A and B sites were shown to correspond to the trigonal and tetragonal sites respectively.[10] Figure 4 shows an example of the site assignments for a given manifold—in this case the D manifold. Table I lists the wavelengths for the absorption (excitation) and fluorescence lines identified by site and observed in the 0.01-mole% CaF_2: Ho^{3+} crystal.

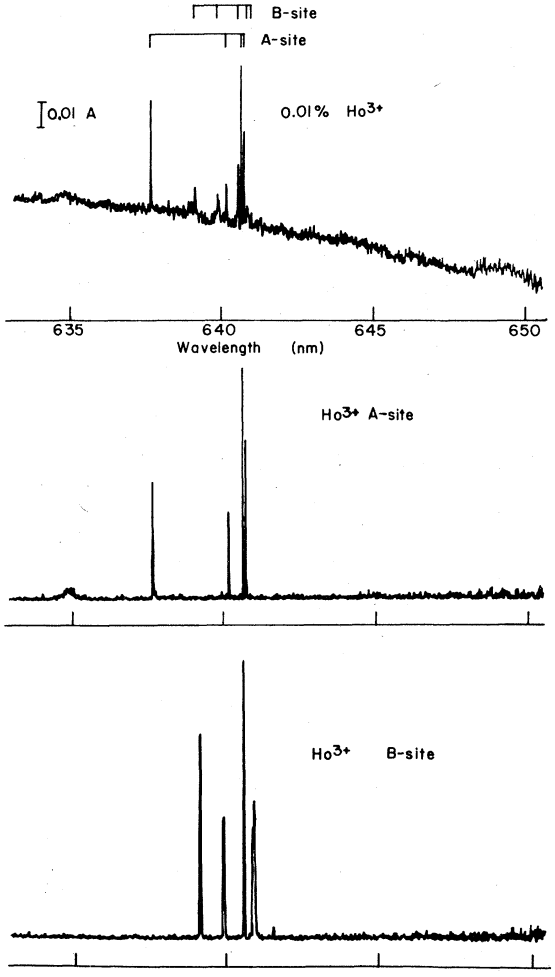

FIG. 4. A and B site excitation spectra and absorption spectrum showing site assignments: ${}^5I_8 \rightarrow {}^5F_5$ ($Z \rightarrow D$). Ordinate in absorbance units (A).

CaF_2: 0.2-mole % Ho^{3+}

The procedure described above is repeated using a CaF_2: 0.2-mole% Ho^{3+} crystal. The absorption spectrum for the 0.2-mole% crystal shown in Fig. 5 is considerably more complex than that of the 0.01-mole% crystal, and has both sharp and broad features. Both the large number of lines and the broad line widths require careful selection of wavelengths used to obtain the single site spectra in order to eliminate overlapping features from different sites. Spectra that are obtained when there is overlap can be recognized because fluorescence lines from Ho^{3+} ions in a particular site must have the same relative intensities regardless of the

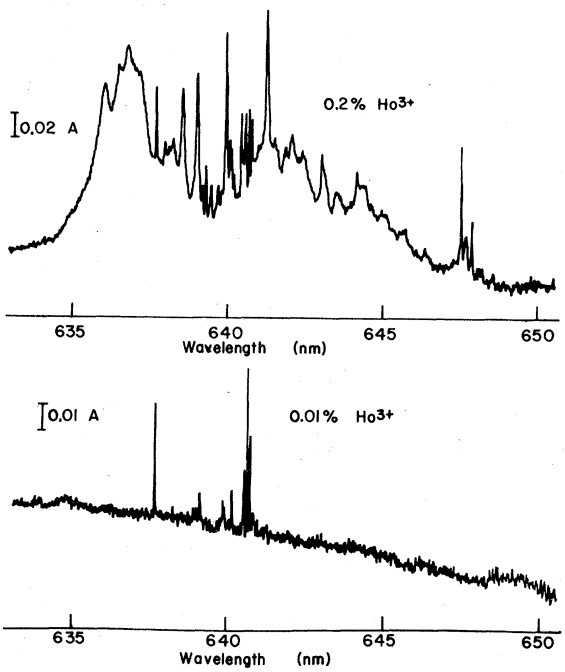

FIG. 5. ${}^5I_8 \rightarrow {}^5F_5$ ($Z \rightarrow D$) absorption spectra of 0.2-mole % Ho^{3+} and 0.01-mole % Ho^{3+} in CaF_2. Ordinate in absorbance units (A).

absorption feature excited. Fluorescence lines from sites that have accidentally overlapping absorption features will have different intensities relative to the site under study depending on the degree of overlap.

The additional lines which appear at the 0.2-mole% Ho^{3+} concentration can be classified into three additional sites labeled C, D, and E. The

TABLE I. Energies of observed transitions in excitation (absorption) and in fluorescence from the single-pair sites. Table key: VS- very strong; S- strong; M- medium; W- weak; VW- very weak; n- narrow; b- broad; s- shoulder present. All transition energies given in cm^{-1} corrected for vacuum.

Excitation (absorption)		Fluorescence	
A site	B site	A site	B site
$^5I_8 \rightarrow {}^5F_5$	(± 0.5 cm^{-1})	$^5F_5 \rightarrow {}^5I_8$	
15 680.8 S n	15 645.6 S n	15 619.4 W n	15 646.1 W n
15 619.9 M n	15 627.3 M n	15 608.0 S n	15 626.0 W n
15 607.9 VS n	15 610.1 S n	15 606.2 S n	15 610.0 S n
15 606.0 VS n	15 603.8 M n	15 528.2 W n	15 603.6 M n
	15 602.2 M n	15 516.7 M n	15 602.8 S n
	15 587.0 W n	15 512.3 S n	15 587.5 M n
		15 489.5 W n	15 576.9 W n
		15 321.7 M b	15 575.5 W n
		15 150.6 W b	15 561.5 W n
		15 135.8 M n	15 546.1 VW n
		15 130.8 M n	15 537.2 VS n
		15 119.4 M n	15 463.7 W n
		15 091.1 W b	15 447.8 W b
			15 425.3 W b
			15 396.9 W b
			15 236.9 W b
$^5I_8 \rightarrow {}^5F_4, {}^5S_2$	(± 0.1 cm^{-1})	$^5F_4, {}^5S_2 \rightarrow {}^5I_8$	
18 886.2 M b	18 772.9 S n	18 612.4 M n	18 565.7 S n
18 833.0 S n	18 750.9 M b	18 528.7 W n	18 538.0 S n
18 772.7 W b	18 712.8 S s	18 515.0 W n	18 535.8 W n
18 749.6 S n	18 687.1 W n	18 481.5 M n	18 500.2 M n
18 725.5 W n	18 659.9 M n	18 468.9 W n	18 426.4 W b
18 714.7 W b	18 641.1 M n	18 135.7 S n	18 387.0 M b
18 657.0 W n	18 636.2 VS n	18 120.9 M n	18 357.0 M b
18 634.3 W n	18 577.6 VS n	18 084.1 M n	18 198.9 M b
18 618.6 M n			18 148.1 S s
18 576.8 W n			
	(± 0.1 cm^{-1})	$^5F_4, {}^5S_2 \rightarrow {}^5I_7$	
		13 339.8 M n	13 360.7 M n
		13 324.1 S n	13 353.5 S n
		13 303.4 W n	13 349.8 M n
		13 263.9 S n	13 347.7 M n
			13 343.6 M n
			13 342.9 W n
			13 329.8 W n
			13 328.0 S n
			13 326.1 M n
			13 323.9 M n
			13 312.9 S n
			13 311.5 W n
			13 293.6 M n
			13 292.2 M n
			13 290.1 M n
			13 284.7 M n

TABLE I. *(Continued)*

Excitation (absorption)		Fluorescence	
A site	*B* site	*A* site	*B* site
$^5I_8 \rightarrow {}^5F_3$	(± 0.3 cm^{-1})	$^5F_3 \rightarrow {}^5I_8$	
20 924.5 M *b*	20 781.6 S *n*	20 780.6 W *n*	20 722.9 W *n*
20 781.6 S *n*	20 773.8 M *n*	20 741.6 S *n*	26 695.8 W *n*
20 780.3 M *n*	20 751.8 M *n*	20 701.9 M *n*	20 684.4 W *n*
20 741.0 M *n*	20 749.5 M *n*	20 614.7 M *n*	20 657.8 W *n*
	20 722.4 S *n*	20 449.6 M *b*	20 649.6 M *n*
	20 695.7 M *n*	20 306.3 W *b*	
	20 687.9 S *n*	20 270.9 W *b*	
	(± 0.3 cm^{-1})	$^5F_3 \rightarrow {}^5I_7$	
		15 488.1 M *n*	15 517.6 M *n*
		15 469.5 S *n*	15 504.0 M *n*
		15 427.8 W *n*	15 496.1 S *n*
		15 411.3 S *n*	15 487.0 S *n*
		15 328.3 S *n*	15 485.1 S *n*
			15 479.4 M *n*
			15 472.2 M *n*
			15 468.7 S *n*
			15 443.1 M *n*
			15 434.0 W *n*
$^5I_8 \rightarrow {}^3K_8$	(± 1 cm^{-1})		
21 653 S *n*	21 536 M *n*		
21 631 M *n*	21 528 W *b*		
21 623 W *n*	21 478 W *n*		
21 552 M *s*	21 447 M *n*		
21 538 W *n*	21 388 M *n*		
21 537 M *n*	21 379 S *n*		
21 458 S *n*			
21 457 W *n*			
21 451 S *n*			
21 449 S *n*			
21 423 W *n*			
21 325 W *n*			
$^5I_8 \rightarrow {}^5F_1, {}^5G_6$	(± 1 cm^{-1})		
22 657 M *n*	22 512 W *b*		
22 607 M *n*	22 469 M *b*		
22 528 M *n*	22 460 M *b*		
22 506 S *n*	22 420 M *b*		
22 478 S *n*	22 400 M *n*		
22 336 S *n*	22 350 M *n*		
22 299 S *n*	22 323 W *b*		
	22 315 W *n*		
	22 305 S *n*		
	22 280 S *n*		
	22 262 S *n*		
	22 257 M *n*		
	22 236 S *n*		

Ho^{3+} ions in these sites have been assigned to clusters of several Ho^{3+} ions and their charge compensations.

The *E*-site designation actually corresponds to a family of discrete sites, differing from each other only very slightly in spectral and temporal characteristics. Representative spectra of these sites are shown in Fig. 6. There are three re-

TABLE II. Energies of observed transitions in excitation (absorption) and in fluorescence from the single-pair sights. Table key: VS- very strong; S- strong; M- medium; W- weak; VW- very weak; *n*- narrow; *b*- broad; *s*- shoulder present. All transition energies given in cm^{-1} corrected for vacuum.

Excitation (absorption) $^5I_8 \rightarrow {}^5F_5$ (±0.5 cm^{-1})					Fluorescence $^5F_5 \rightarrow {}^5I_8$				
C	*D*	*E*-1	*E*-2	*E*-3	*C*	*D*	*E*-1	*E*-2	*E*-3
15 666.6 M *n*	15 701.7 M *n*	15 704.8 M *b*	15 722.9 M *b*	15 715.0 W *b*	15 633.4 W *b*	15 627.0 W *n*	15 444.4 S *n*	15 447.3 S *n*	15 438.8 S *n*
15 659.5 S *n*	15 692.8 M *n*	15 648.9 W *n*	15 693.8 M *b*	15 700.2 W *b*	15 619.5 W *b*	15 621.6 M *n*	15 434.6 W *b*	15 431.4 M *n*	15 422.7 M *n*
15 648.5 S *n*	15 688.2 M *n*	15 570.1 M *n*	15 611.1 W *n*	15 648.1 VW *b*	15 608.1 W *b*	15 617.4 M *n*		15 427.0 W *n*	15 416.7 W *n*
15 637.7 M *n*	15 672.7 S *n*	15 565.6 M *n*	15 602.6 M *b*	15 626.1 VW *b*	15 599.1 S *n*	15 614.0 VS *n*		15 423.4 W *n*	15 412.2 W *n*
15 625.7 S *n*	15 670.0 M *n*	15 444.1 S *n*	15 595.9 M *n*	15 611.0 VW *b*	15 592.7 W *b*	15 606.5 M *n*		15 365.0 M *n*	15 397.8 W *b*
15 622.3 M *n*	15 644.4 S *n*		15 577.6 M *b*	15 604.1 VW *b*	15 582.5 S *n*	15 605.4 M *n*			
15 612.8 M *n*	15 642.0 VS *n*		15 550.7 M *b*	15 594.4 W *b*	15 560.4 S *n*	15 599.4 M *n*			
15 611.0 M *n*	15 632.5 M *n*		15 527.1 M *s*	15 589.0 W *b*	15 559.6 S *n*	15 598.2 M *n*			
15 594.6 S *n*	15 629.3 W *n*		15 520.8 W *n*	15 577.1 W *b*	15 548.8 W *b*	15 594.8 M *n*			
15 581.1 M *n*	15 627.2 M *n*		15 489.5 W *n*	15 564.0 W *b*	15 535.2 W *b*	15 582.8 S *n*			
15 559.8 M *n*	15 621.6 S *n*		15 447.6 S *n*	15 540.6 VW *b*	15 526.3 W *b*	15 575.4 M *n*			
	15 617.2 M *n*		15 431.6 M *n*	15 518.8 W *b*	15 516.7 S *n*	15 561.8 M *n*			
	15 614.4 VS *n*			15 503.4 VW *b*	15 498.2 W *b*	15 554.2 M *n*			
	15 606.0 W *n*			15 472.8 W *n*	15 464.3 M *b*	15 544.1 W *n*			
	15 598.9 W *n*			15 439.0 S *n*	15 418.3 M *b*	15 532.3 M *n*			
	15 593.2 W *n*			15 422.7 W *n*		15 526.4 S *n*			
						15 496.2 W *n*			

$^5I_8 \rightarrow {}^5F_4, {}^5S_2$ (±0.5 cm^{-1})					$^5F_4, {}^5S_2 \rightarrow {}^5I_8$				
C	*D*	*E*-1	*E*-2	*E*-3	*C*	*D*	*E*-1	*E*-2	*E*-3
18 794.1 S *n*	18 823.0 S *n*	The *E*-family sites are responsible for broad background absorption between 18 860 cm^{-1} and 18 620 cm^{-1} and between 18 600 cm^{-1} and 18 510 cm^{-1}				Fluorescence not observed			
18 779.8 W *b*	18 808.1 M *n*								
18 767.7 M *s*	18 807.0 M *n*								
18 745.9 M *n*	18 767.0 W *n*								
18 740.5 S *n*	18 762.8 W *n*								
18 731.9 W *n*	18 754.3 S *n*								
18 726.1 S *n*	18 747.9 M *n*								
18 716.1 W *b*	18 739.8 W *n*								
18 705.4 W *n*	18 706.3 S *n*								
18 690.1 W *n*	18 677.0 M *n*								
18 673.3 S *n*	18 665.8 M *n*								
18 656.5 S *n*	18 662.6 W *n*								
18 643.1 M *n*	18 527.2 W *n*								
18 629.3 M *n*	18 514.9 S *n*								
18 622.2 W *n*	18 499.4 W *n*								
18 609.2 W *n*									
18 597.4 M *n*									
18 594.4 W *n*									
18 590.3 S *n*									

TABLE II. *(Continued)*

Excitation (absorption) $^5I_8 \rightarrow {}^5F_4, {}^5S_2$ (±0.5 cm^{-1})					Fluorescence $^5F_4, {}^5S_2 \rightarrow {}^5I_8$				
C	*D*	*E*-1	*E*-2	*E*-3	*C*	*D*	*E*-1	*E*-2	*E*-3
18 583.0 M *n*									
18 575.6 M *n*									
18 563.9 W *n*									
18 556.6 W *n*									
$^5I_8 \rightarrow {}^5F_3$ (±0.5 cm^{-1})					$^5F_3 \rightarrow {}^5I_8$				
C	*D*	*E*-1	*E*-2	*E*-3	*C*	*D*	*E*-1	*E*-2	*E*-3
20 818.9 S *n*	20 854.9 M *n*	The *E*-family sites are responsible for broad background absorption between 20 820 cm^{-1} and 20 710 cm^{-1} and between 20 700 cm^{-1} and 20 610 cm^{-1}			20 737.0 W *n*	20 756 M *n*	20 202 S *b*	20 324 W *b*	20 193 M *b*
20 803.2 M *n*	20 837.5 W *n*				20 725.9 W *n*	20 738 S *n*	20 157 M *b*	20 198 S *b*	20 155 S *b*
20 788.0 M *n*	20 827.9 W *n*				20 722.8 W *n*	20 716 M *n*		20 158 M *b*	
20 782.6 W *n*	20 775.1 M *n*				20 715.8 W *n*	20 711 W *n*			
20 757.5 M *n*	20 767.8 M *n*				20 705.5 M *n*	20 691 S *n*			
20 741.0 M *n*	20 759.2 W *n*				20 701.1 M *n*	20 665 W *n*			
20 736.1 S *n*	20 749.3 S *n*				20 695.7 S *n*	20 661 M *n*			
20 730.0 M *n*	20 733.8 M *n*				20 671.3 W *n*	20 513 W *b*			
20 726.3 M *n*					20 662.2 M *n*	20 274 M *b*			
20 721.6 M *n*					20 654.8 S *n*				
20 715.2 M *n*					20 606.0 W *b*				
20 704.7 W *n*					20 537.8 M *b*				
20 700.6 W *n*					20 391.6 W *b*				
20 694.7 M *n*					20 347.7 W *b*				
					20 302.2 W *b*				
$^5I_8 \rightarrow {}^3K_8$ (0.1 cm^{-1})					$^3K_8 \rightarrow {}^5I_8$				
C	*D*	*E*-1	*E*-2	*E*-3	*C*	*D*	*E*-1	*E*-2	*E*-3
21 556.7 S *s*	21 548.5 W *b*	The *E*-family sites are responsible for broad background absorption between 21 680 cm^{-1} and 21 360 cm^{-1}			Fluorescence not observed				
21 546.8 M *n*	21 525.7 W *b*								
21 542.7 M *n*	21 507.6 W *n*								
21 537.8 M *n*	21 486.4 W *b*								
21 532.7 W *n*	21 455.1 W *b*								
21 528.8 W *n*	21 444.4 W *n*								
21 516.8 VW *n*	21 437.3 W *n*								
21 508.4 W *n*	21 437.2 M *s*								
21 501.5 W *b*	21 426.0 S *n*								
21 489.5 W *s*	21 419.8 M *n*								
21 473.9 W *n*	21 416.0 W *n*								
21 469.3 M *n*	21 412.8 W *b*								
21 461.5 S *n*	21 407.0 M *n*								
21 454.2 W *n*	21 399.2 M *n*								

TABLE II. *(Continued)*

Excitation (absorption) $^5I_8 \rightarrow {}^3K_8$ (±0.1 cm^{-1})					Fluorescence $^3K_8 \rightarrow {}^5I_8$				
C	*D*	*E*-1	*E*-2	*E*-3	*C*	*D*	*E*-1	*E*-2	*E*-3
21 446.1 W *n*	21 392.6 W *n*								
21 443.3 W *n*	21 366.4 S *n*								
21 438.0 W *n*	21 355.1 M *n*								
21 404.8 M *n*									
21 399.2 S *n*									
21 396.0 S *n*									
21 393.3 S *n*									
21 389.8 W *n*									
21 384.2 W *n*									
21 378.0 M *n*									
21 368.8 W *b*									
21 364.1 W *n*									
		$^5I_8 \rightarrow {}^5F_1, {}^5G_6$ (±0.2 cm^{-1})					$^5F_1, {}^5G_6 \rightarrow {}^5I_8$		
C	*D*	*E*-1	*E*-2	*E*-3	*C*	*D*	*E*-1	*E*-2	*E*-3
22 381.7 M *n*	22 687.4 W *b*	22 178.4 S *n*	22 195.4 W *n*	22 172.0 S *n*			Fluorescence not observed		
22 354.9 S *n*	22 640.1 W *b*		22 182.6 S *n*	22 168.4 S *n*					
22 334.0 S *s*	22 599.2 W *b*		22 175.0 S *n*						
22 326.4 M *n*	22 583.3 W *b*		22 161.2 W *n*						
22 310.4 M *s*	22 473.7 M *b*								
22 297.2 S *n*	22 444.4 W *b*	*E*-family sites also contribute broad background absorption between 22 460 cm^{-1} and 22 150 cm^{-1}							
22 294.9 S *n*	22 402.9 W *n*								
22 281.1 S *n*	22 392.6 W *n*								
22 267.9 W *s*	22 376.2 M *n*								
22 264.5 W *s*	22 353.1 W *n*								
22 259.8 S *n*	22 348.7 W *n*								
22 244.9 M *s*	22 340.0 M *n*								
	22 329.4 W *n*								
	22 321.2 W *n*								
	22 318.4 M *n*								
	22 306.1 M *n*								
	22 289.5 S *n*								
	22 281.7 W *n*								
	22 274.1 W *n*								
	22 272.1 W *n*								
	22 269.1 S *n*								
	22 255.1 M *n*								

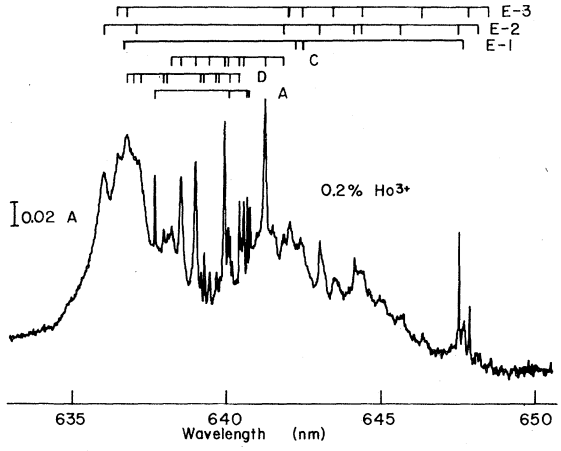

FIG. 6. $Z \rightarrow D$ absorption spectrum of 0.2-mole % Ho^{3+} in CaF_2 showing site assignments. The ordinate is in absorbance units (A).

solvable, individual sites within this family labeled E-1, E-2, and E-3, plus additional unresolved sites of weaker intensity. This family of sites distinguishes itself from all the other sites because its spectrum appears at longer wavelength, in both excitation and fluorescence, than the other sites and has a shorter lifetime than the other cluster sites of the same manifold. The E-family sites are also responsible for the majority of the broad background present in the absorption spectra of the 0.2-mole % Ho^{3+} crystal. Table II lists the wavelengths of the excitation and fluorescence lines for the various sites in the CaF_2: 0.2-mole % Ho^{3+} crystal.

Note that in Table II no fluorescence originating from the E manifold is listed for any of the cluster sites, even though fluorescence from these sites is observed from the D manifold. The absence of fluorescence from the E manifold is due to efficient, nonradiative decay processes which occur between clustered Ho^{3+} ions, but cannot occur for Ho^{3+} ions in the isolated sites A and B. This phenomenon will be discussed in greater detail later.

The absorption (excitation) lines from the A and B sites are also present in the spectra of the 0.2-mole % Ho^{3+} crystal, but the spectra are dominated by the features arising from the cluser sites. The transitions for the A and B sites tabulated in Table I remain unchanged for the higher concentration crystal.

Single-ion site fluorescence decay characteristics

The temporal behavior of the A and B sites fluorescence was studied in the CaF_2: 0.01-mole % Ho^{3+} sample. The fluorescence decay behavior observed can be explained in all cases by unique relaxation rates and sequential decay between manifolds for all of the manifolds studied. The relaxation rate is the sum of the radiative rate from a manifold and the nonradiative relaxation rate by multiphonon emission from a manifold to the next lower manifold. The lifetimes determined for the different manifolds for the A and B sites are given in Table III. They were obtained both by direct excitation of the manifold and by indirect excitation via higher manifolds which then relax to the manifold in question. In the latter case, the lifetimes of the intermediate levels must also be considered. The data for both direct and indirect excitation is consistent and provided in Table III.

TABLE III. Manifold lifetimes of single-pair sights (μsec).

Manifold	Site A	Site B
D	72.3 (±0.6)	114 (±1)
E	1291 (±26)	534 (±10)
F	5.26 (±0.1)	5.20 (±0.05)

Cluster site fluorescence decay characteristics

The clustered Ho^{3+} ions in the 0.2-mole % crystals exhibit an additional nonradiative decay process documented previously in Er^{3+} clusters by Tallant, Miller, and Wright.[13] The close proximity of the Ho^{3+} ions in the clusters permits efficient ion-pair energy transfer between adjacent ions. Often, a nonresonant energy transfer is more efficient than a simple multiphoton relaxation because of the exponential rate dependence on the number of phonons involved in each decay step. The contribution which ion-pair energy-transfer processes make to the overall relaxation process is best observed when the E manifold is excited and fluorescence is monitored from the E and D manifolds.

As Table III shows, energy in the sigle-ion A site decays from the E manifold to the D manifold via multiphonon relaxation in 1.29 msec. When fluorescence from the D manifold is monitored, a rise time of 72 μsec, characteristic of the lifetime of the D manifold, is observed and followed by the 1.29 msec delay. Additionally, the fluorescence from the D manifold is several orders of magnitude weaker when it is excited indirectly via the E manifold. This weaker fluorescence is due to the large 3000 cm^{-1} energy gap between the E and D manifolds which prevents efficient nonradiative relaxation by multiphonon processes. The single-ion B site behaves in a similar fashion.

Exactly opposite behavior is observed for the C, D, and E cluster sites in Table IV. No fluor-

TABLE IV. *D*-manifold lifetimes of cluster sites (μsec).

Site		
C	*D*	*E* (all)
101.3 (±0.9)	125 (±2)	17.3–19.1 (±1.3)

escence is detected from the *E* manifold after direct excitation, while the fluorescence from *D* is very strong and decays rapidly (125, 100, and 20 μsec for the *C*, *D*, and *E* sites, respectively). Figure 7 shows a shorthand representation of the ion-pair relaxations responsible for this behavior. One ion in the cluster can relax by transferring energy to an adjacent ion, exciting it to a higher energy manifold, with any difference in energy being dissipated as lattice phonons. A possible first step to explain the decay from the *E* manifold is for the excited ion to decay to the *Y* (or *C*) manifold, simultaneously transferring the bulk of the lost energy to the adjacent ion which is excited from the ground state to the *C* (or *Y*) manifold. This decay step requires dissipation of only 200 cm^{-1} of energy as lattice phonons, much less than the 3000 cm^{-1} required by direct relaxation from $E \rightarrow D$. The second step would involve a second energy transfer between ions, resulting with both ions in the *A* manifolds ($A+A$ level). The third step would result with one ion in the *Y* manifold and the other in the *B* manifold ($Y+B$ level). Finally, one ion would end up in the *D* manifold and the adjacent ion in the ground state. The overall result is the same as the multiphonon process of the single-ion sites, but the energy gaps for the four steps are 200 cm^{-1}, 1000 cm^{-1}, 1000 cm^{-1}, and 800 cm^{-1} instead of the 3000 cm^{-1} gap of the multiphonon process. Because the efficiency of the process depends exponentially on the energy mismatch, the process with several, smaller mismatches is expected to be favored over one with a single, large mismatch.

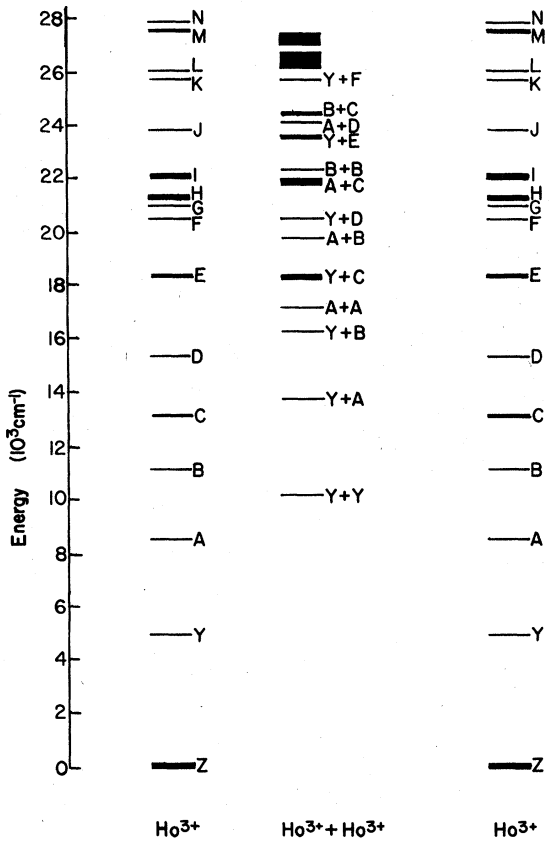

FIG. 7. Energy-level diagram with schematic representation of ion-pair levels for two adjacent Ho^{3+} ions.

Because the energy gap from *E* to ($Y+C$) is only 200 cm^{-1}, the nonradiative process is very efficient and no fluorescence is seen from the *E* manifold. The overall ion-pair decay scheme also accounts for the strong *D* manifold fluorescence when the *E* manifold is excited. The efficiency of the ion-pair process is also reflected in the very fast (< 10 μsec) rise on the *D* manifold fluorescence, corresponding to a very short *E* manifold lifetime. The relaxation rates for the *C*, *D*, and *E* sites are listed in Table IV.

Up conversion

In addition to facilitating energy decay in cluster-site ions, ion-pair energy transfer can also result in the efficient population of higher energy levels. This up conversion can occur when two or more ions of a cluster site are simultaneously excited. If one of the ions relaxes by energy transfer to the adjacent excited ion, the adjacent ion can be excited to a higher manifold than would be possible by direct photon absorption. Any energy mismatch in this process is again absorbed by lattice phonons.

This up conversion of excitation energy has been used to aid in identifying and characterizing the cluster sites. As was discussed earlier, no fluorescence is observed from the *E* level of cluster sites when either the *E* manifold or higher manifolds are excited. However, the up conversion that results when two ions in a cluster are excited to the *D* manifold produces not only fluorescence from the *J* and *F* manifolds, but also from the previously nonfluorescent *E* manifold. The *E* manifold fluorescence that results from this excitation arises because the adjacent ion in the cluster has not yet relaxed to the ground level, which is necessary for the previously outlined energy-transfer process that quenches *E* manifold fluorescence.

TABLE V. Energies of observed fluorescence transitions from the E manifold pumped by up conversion from the D manifold. Table key: VS-very strong; S- strong; M- medium; W- weak; VW- very weak; n- narrow; b- broad; s- shoulder present. All transition energies given in cm^{-1} corrected for vacuum.

C site	
$^5S_2$, $^5F_4 \rightarrow {}^5I_8$	$^5S_2$, $^5F_4 \rightarrow {}^5I_7$
18 588.3 W n	13 365.9 M n
18 580.5 M n	13 353.9 S n
18 573.2 W n	13 347.9 W n
18 565.3 M n	13 342.5 M n
18 551.0 W n	13 339.2 M n
18 544.0 S n	13 337.5 M n
18 522.7 VW n	13 333.2 W n
18 514.9 W n	13 329.5 W n
18 506.4 W b	13 326.9 M n
18 499.1 M n	13 323.9 M n
18 479.4 VW b	13 315.5 M n
18 437.8 W b	13 313.5 M n
18 366.4 M b	13 307.9 W n
18 335.7 M b	13 302.9 M n
18 197.9 S b	13 300.3 M b
18 189.4 M b	13 293.0 M b
18 142.7 S b	13 281.1 M b
	13 266.2 W b

The E manifold is then "forced" to fluoresce until the manifold is emptied by multiphonon decay or an energy-transfer decay process becomes available. The fluorescence lines obtained for E manifold fluorescence for the cluster site excited by up conversion are listed in Table V.

Doubly-doped crystals

With this new information on CaF_2: Ho^{3+} along with data from previous work done in our laboratory on Er^{3+}-doped CaF_2,[10,13] a study of a double-doped CaF_2 crystal containing both Ho^{3+} and Er^{3+} was undertaken. The goals for this study were (1) to provide additional proof of the existence and importance of dimers and clusters at higher dopant concentrations, (2) to correlate the spectra of dimer and cluster sites among different rare-earth dopants, and (3) to investigate the changes that occur in site distributions as the ionic radii change from dopant to dopant.

By doping one ion at a low concentration (0.01-mole%) and the other at a higher concentration (0.2-mole%), one should obtain a nearly total incorporation of the lower concentration ions into the clusters of the higher concentration ions. Since one could then excite ions of one species and observe fluorescence from the second ionic species, a correlation could be established between the spectra of the different ions. Er^{3+} was chosen as the second dopant ion because of the large amount of knowledge available about it.

Mixed Ho^{3+}-Er^{3+} clusters are difficult to study, however, because many of the Ho^{3+} energy levels fall at the same energy as the Er^{3+} energy levels (Fig. 8). Figure 9 shows, for example, the absorption spectrum of the F manifold of Ho^{3+} in a CaF_2: 0.2-mole% Ho^{3+} crystal, along with the G manifolds of Er^{3+} in a CaF_2: 0.01-mole% Er^{3+} crystal. This coincidence of Er^{3+} and Ho^{3+} lines prevents the excitation of one ion without simultaneous excitation of the other ion. Since the Ho^{3+} is present at the higher concentration, an excitation spectrum taken, monitoring Ho^{3+} fluorescence, exhibits only the Ho^{3+} excitation lines of the Ho^{3+} clusters while any Er^{3+} excitation lines are masked. The same problem arises for the majority of excitation (fluorescence) cases in the Ho^{3+}-Er^{3+} mixed crystal.

There are, however, two spectral regions where this problem can be overcome. The F manifold of Er^{3+} is sufficiently higher in energy than the Ho^{3+}

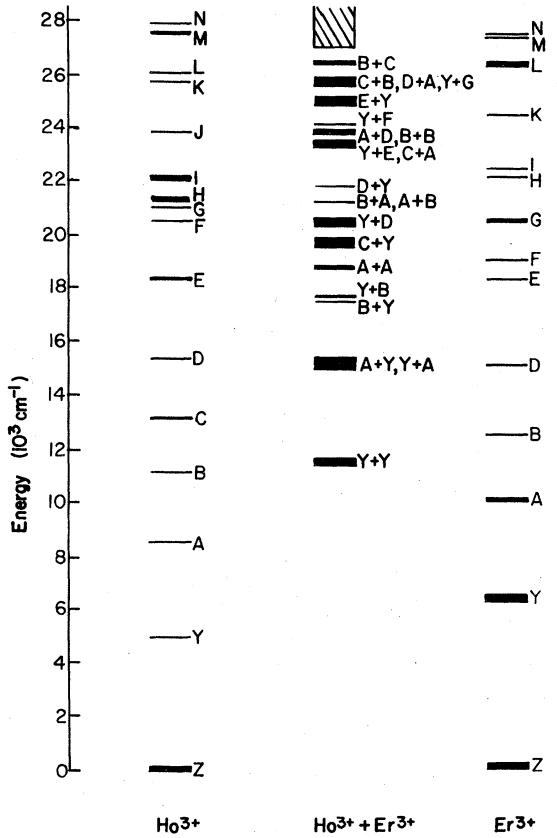

FIG. 8. Energy-level diagram with schematic representation of ion-pair levels for adjacent Ho^{3+} and Er^{3+} ions.

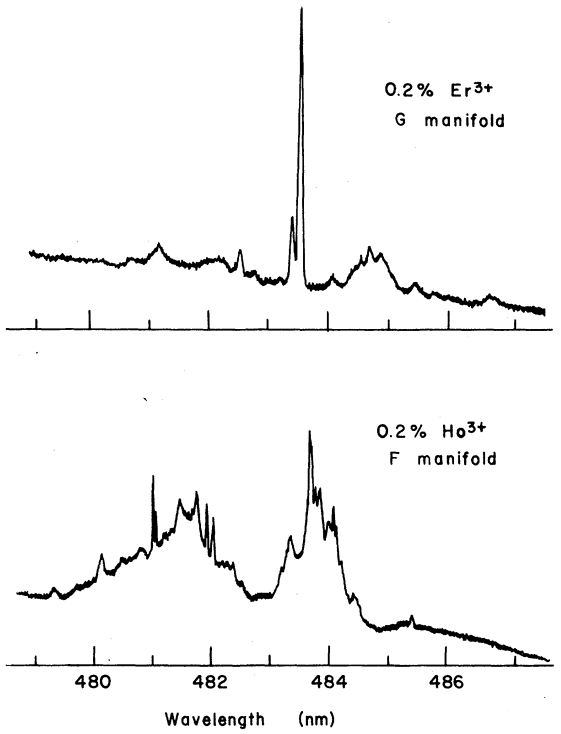

FIG. 9. Absorption spectra of the G manifold of 0.2-mole % Er^{3+} in CaF_2 and the F manifold of 0.2-mole % Ho^{3+} in CaF_2 showing the large degree of overlap typical of the energy levels in mixed crystals of Er^{3+} and Ho^{3+}.

E manifold to allow some degree of selective excitation. Also, the $E \rightarrow Y$ fluorescence of Ho^{3+} is completely separate from the $E \rightarrow Y$ fluorescence of Er^{3+}.

The absorption spectra obtained for a series of CaF_2 crystals doped with (1) 0.01-mole % Er^{3+}, (2) 0.01-mole % Er^{3+} and 0.2-mole % Ho^{3+}, and (3) 0.2-mole % Er^{3+} are shown in Fig. 10. In spectrum (b) the Er^{3+} lines characteristic of single Er^{3+} ions disappear, while Er^{3+} lines characteristic of clustered ions appear. The cluster sites are the same ones observed in the higher concentration 0.2-mole % Er^{3+} crystals. This change is caused by the incorporation of the Er^{3+} into the Ho^{3+} clusters present at the high Ho^{3+} concentration.

Although there is still spectral overlap between sites in this experiment, it can be avoided by time resolution of the fluorescent transients. Because the fluorescent lifetime of the Er^{3+}-Ho^{3+} dimer is very short compared with that of the interfering Ho^{3+} single site fluorescence, a short detection window would emphasize the dimer fluorescence as shown in Fig. 11.

The excitation spectrum obtained in the mixed ion experiment was that of Er^{3+} C site. The corresponding fluorescence spectrum was that of the

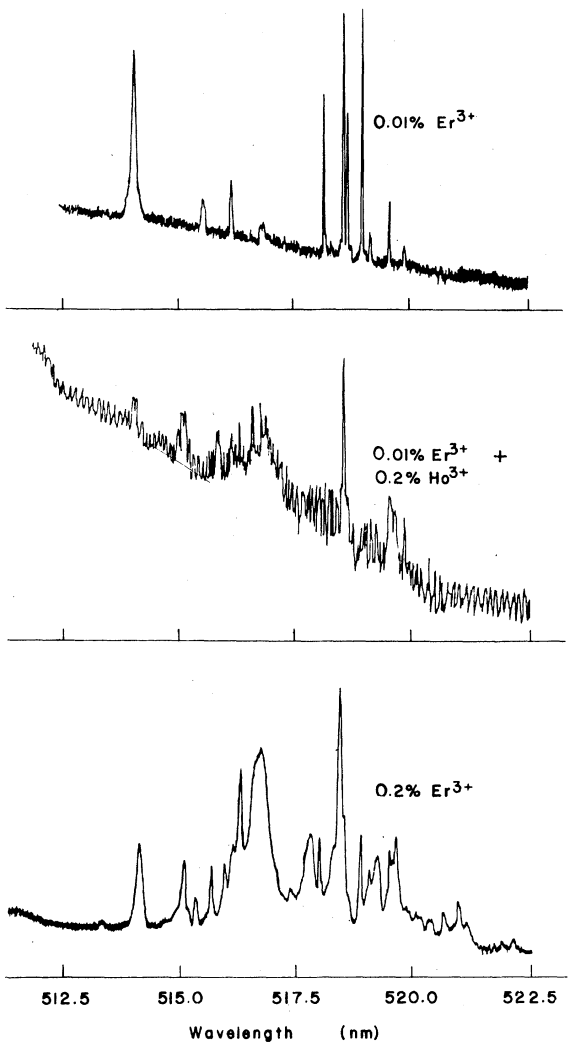

FIG. 10. Absorption spectrum of the $^2H_{11/2}$ manifold of Er^{3+} in CaF_2 crystals: 0.01-mole % Er^{3+} (top); 0.01-mole % Er^{3+}, 0.2-mole % Ho^{3+} (middle); and 0.2-mole % Er^{3+} (bottom).

Ho^{3+} C site, previously only obtainable using upconversion excitation. Because the ion-pair processes available in the Ho^{3+} dimers are not present in the Ho^{3+}-Er^{3+} mixed crystal, an efficient nonradiative decay path is not present and the $E \rightarrow Y$ fluorescence is observable. Similar evidence to show relationships between the Ho^{3+} D and E sites and Er^{3+} $D1$ and $D2$ sites was not observed.

CONCLUSIONS

The sites in CaF_2: Ho^{3+} are very similar to those previously observed in CaF_2: Er^{3+}. At low concentrations, the Ho^{3+} ions reside in two crystallographic sites (labeled A and B) which contain single Ho^{3+} ions and probably correspond to the

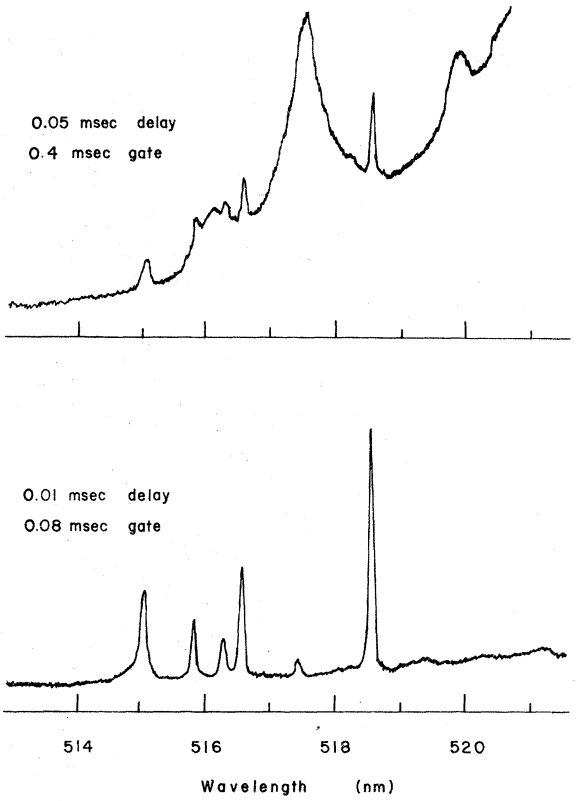

FIG. 11. Excitation spectra of mixed Ho^{3+}, Er^{3+} crystals showing how Ho^{3+} single-ion site fluorescence can be discriminated against temporally to observe more clearly the fluorescence due to energy transfer between dissimilar dimer sites.

tetragonal and trigonal sites. At concentrations above ca. 0.05-mole%, these sites decrease markedly in importance and a series of new lines appear which correspond to a number of sites which are associated with clustering of ions (these sites are labeled *C*, *D*, and *E*, where *E* represents many similar sites). Energy transfer occurs very efficiently between the ions in these clusters and both ion-pair decay and up-conversion processes are observed. The energy transfer was used in studies of Ho^{3+}, CaF_2: Er^{3+} mixed crystals to identify the spectral features of each dopant which were associated with energy transfer between Ho^{3+} and Er^{3+}, and to therefore define the correspondence between Er^{3+} sites that have been previously identified with the Ho^{3+} sites observed in this study. It was found that the *C* site of Er^{3+} corresponds to the *C* site of Ho^{3+}. This site is particularly important in a fluorite-structure material because it corresponds to a site where additional fluoride-interstitial ions have been scavenged by the clusters to form negatively charged defect structures.[11] This scavenging is largely responsible for determining the positions of the defect equilibria and for explaining the anomalous behavior that has been observed in studying the populations of different defects.

ACKNOWLEDGMENT

This research was supported by the National Science Foundation under Grant Nos. DMR77-07765 and DMR79-06788.

[1]J. Sierro, Phys. Lett. 4, 178 (1963).
[2]U. Ranon and A. Yariv, Phys. Lett. 9, 17 (1964).
[3]M. R. Brown, K. G. Roots, J. M. Williams, W. A. Shand, G. Grover, and H. F. Kay, J. Chem. Phys. 50, 891 (1969).
[4]F. K. Fong, R. L. Ford, and R. H. Heist, Phys. Rev. B 2, 4202 (1970).
[5]M. J. Weber and R. W. Bierig, Phys. Rev. 134, A1492 (1964).
[6]C. R. A. Catlow, J. Phys. C 9, 1845 (1976).
[7]S. L. Naberhuis and F. K. Fong, J. Chem. Phys. 56, 1174 (1972).
[8]R. J. Booth, M. R. Mustafa, and B. R. McGarvey, Phys. Rev. B 17, 4150 (1978).
[9]R. Capelletti, E. Okuno, G. E. Matthews, and J. H. Crawford, Jr., Phys. Status Solidi A47, 617 (1978).
[10]D. R. Tallant and J. C. Wright, J. Chem. Phys. 63, 2074 (1975).
[11]D. S. Moore and J. C. Wright (in press).
[12]F. K. Fong, J. Chem. Phys. 64, 4243 (1976).
[13]D. R. Tallant, M. P. Miller, and J. C. Wright, J. Chem. Phys. 65, 510 (1976).
[14]M. P. Miller, Ph.D. thesis, University of Wisconsin-Madison, 1978 (University Microfilms, Ann Arbor, Mich.).
[15]J. C. Wright, *Applications of Lasers to Chemical Problems*, edited by T. R. Evans (Wiley-Interscience, New York, to be published).
[16]J. C. Wright, *Topics in Applied Physics, Radiationless Processes in Molecules and Condensed Phases*, edited by F. K. Fong (Springer, Berlin, 1976), Vol. 15.
[17]D. R. Tallant, D. S. Moore, and J. C. Wright, J. Chem. Phys. 67, 2897 (1977).